Journal of Materials Chemistry C

ROYAL SOCIETY OF CHEMISTRY

PAPER

View Article Online
View Journal | View Issue

Cite this: J. Mater. Chem. C, 2023, 11, 2880

Multi-stimuli responsive (L-tartrato)oxovanadium(V) complex salt with ferroelectric switching and thermistor properties†

Marko Dunatov, Andreas Puškarić and Lidija Androš Dubraja *

Molecular materials that respond to external triggers and the environment by changing certain properties are currently a very active area of research and are being considered for use in devices. The responsiveness of these highly organized structures is the result of flexible structural arrangements, which in most cases are controlled by non-covalent interactions. Here, we report the exceptional structural flexibility of a complex salt with tetraethylammonium cations, (L-tartrato)oxovanadium(V) anions and water molecules of crystallization. This compound undergoes multiple crystal transformations from the undecahydrate phase to the dehydrated phase triggered by changes in humidity and temperature. The structural transformations are characterized by single-crystal X-ray diffraction, powder X-ray diffraction and infrared spectroscopy at variable temperature and humidity and by thermal analysis. The dynamics of the structural transformations occurring in this tetraethylammonium (L-tartrato)oxovanadium(V) system indicates a low energy barrier for reversible release and uptake of water molecules from air. During these transformations, which occur over a very narrow temperature and humidity range, the compound changes from the non-polar $P2_12_12_1$ structure to the polar $P2_1$, $C2$ and $P2$ structures. The structural transformations are accompanied by significant changes in the electrical behaviour of the material: from proton conductivity in the non-polar $P2_12_12_1$ phase to ferroelectricity in the $P2_1$ phase at room temperature, and thermistor behaviour in the temperature range of 313–333 K. In addition, the optical properties of the material, which exhibits pleochroism and photoresponsive behaviour, were investigated using UV-vis diffuse reflectance spectroscopy.

Received 28th November 2022,
Accepted 16th January 2023

DOI: 10.1039/d2tc05064a

rsc.li/materials-c

Introduction

Compounds and complexes of tartaric acid have been studied for centuries, and yet the number of tartrato transition metal complexes is not very large (less than 300 deposits in the CSD).[1,2] This may be related to the rather complex behaviour of this seemingly simple α-hydroxycarboxylic acid, which depends strongly on the experimental conditions, and to the stability problems that some of the tartrato complexes exhibit in the solid state.[3–7] This is also one of the reasons why the solution chemistry of the tartrato complexes has been studied much more thoroughly than the solid state using various methods, *i.e.*, UV-vis spectroscopy, conductometry, cryoscopy, infrared spectroscopy, NMR spectroscopy, polarography, and cyclic voltammetry.[1,3–7] Considering its availability, low cost, nontoxicity, and natural occurrence in the enantiomeric form, L-(+)-tartaric acid ($C_4H_6O_6$) could find much wider application in the development and preparation of inorganic–organic materials as chiral building units.

The complexation of vanadium(V) with L-tartaric acid is pH dependent, and two different forms can be obtained (Scheme 1a and b): the tetranuclear $[V_4O_8(L\text{-tart})_2]^{4-}$ anion,[7–9] and the less stable dinuclear $[V_2O_4(L\text{-tartH}_2)_2]^{2-}$ anion[10] formed in acidic solutions [L-tart = $(C_4H_2O_6)^{4-}$; L-tartH$_2$ = $(C_4H_4O_6)^{2-}$]. In addition to these two forms, the use of racemic DL-tartaric acid gives the $[V_2O_2(D\text{-tart})(L\text{-tart})]^{2-}$ anion,[10] which was isolated in the solid state (Scheme 1c). Complexes of oxovanadium(IV) with L-, D-, or DL-tartaric acid occur only in the dimeric form as the $[V_2O_2(tart)_2]^{4-}$ anion,[11,12] in which each fully deprotonated tartrate residue forms two chelate rings to two vanadium(IV) ions, similar to the structure shown in Scheme 1c. Due to the diversity of coordination topologies and nuclearities of (L-tartrato)oxovanadium complex anions, they provide a good platform for chiral building blocks that can potentially be used to prepare compounds with polar crystal structures of interest

Ruđer Bošković Institute, Bijenička cesta 54, 10000 Zagreb, Croatia.
E-mail: lidija.andros@irb.hr; Tel: +385 1 4561184

† Electronic supplementary information (ESI) available: Single-crystal XRD data (Tables S1, S3 and S4); PXRD data (Table S2 and Fig. S1–S6); TG/DTA results (Fig. S8); pleochroism in crystals (Fig. S7); and resistivity measurements (Fig. S9). CCDC 2221444. For ESI and crystallographic data in CIF or other electronic format see DOI: https://doi.org/10.1039/d2tc05064a

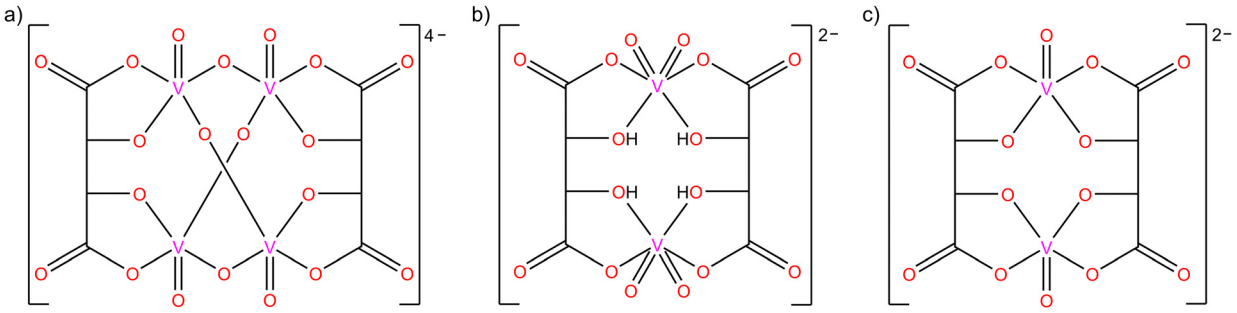

Scheme 1 Different (tartrato)oxovanadium(v) anions: (a) $[V_4O_8(\text{L-tart})_2]^{4-}$, (b) $[V_2O_4(\text{L-tartH}_2)_2]^{2-}$, and (c) $[V_2O_2(\text{D-tart})(\text{L-tart})]^{2-}$.

for application in nonlinear optics, ferroelectrics, and other switchable dielectrics.[8,13–15]

In this work, we have focused on the preparation of a dominant and stable tetranuclear $[V_4O_8(\text{L-tart})_2]^{4-}$ anion that reacts with tetraethylammonium cations $(TEA)^+$ to give a complex salt $(TEA)_4[V_4O_8(\text{L-tart})_2]$. The investigated compound coexists in several hydrate phases and undergoes reversible crystal transformation from the undecahydrate phase to the completely dehydrated phase, through multiple solid state transformations triggered by changes in humidity and temperature. The structural transformations were followed by *in situ* infrared spectroscopy and powder X-ray diffraction, as well as by thermal analysis. The process of crystal transformation from the new undecahydrate phase $(TEA)_4[V_4O_8(\text{L-tart})_2]\cdot 11H_2O$ (**1·11H$_2$O**) to the previously known hexahydrate phase $(TEA)_4[V_4O_8(\text{L-tart})_2]\cdot 6H_2O$ (**1·6H$_2$O**)[7] is followed by a symmetry breakdown from the non-polar orthorhombic $P2_12_12_1$ space group to the polar monoclinic $P2_1$ space group. The polar phase **1·6H$_2$O** is ferroelectric and exhibits a switchable spontaneous polarization under an external electric field at room temperature. Interestingly, the first ferroelectric crystal discovered by Valasek in 1920 was also a tartrate-based system, potassium sodium tartrate tetrahydrate (Rochelle salt), but not many ferroelectric tartrate compounds have been mentioned since.[16,17] One of the few ferroelectric tartrates is the supramolecular adduct of 1,4-diazabicyclo[2.2.2]octane-*N*,*N*′-dioxide and L-tartaric acid,[18] and a hydrogen-bonded ionic co-crystal with imidazole and L-tartaric acid.[19] Apart from the ferroelectric properties, the studied $(TEA)_4[V_4O_8(\text{L-tart})_2]$ compound exhibits other properties induced by external stimuli, such as the temperature- and humidity-induced electrical responses and optical properties dependent on irradiation with visible light. These properties were investigated using chronoamperometric measurements and UV-vis diffuse reflectance spectroscopy.

Experimental

Synthetic procedure

Tetraethylammonium hydroxide (TEAOH) solution 35 wt% in water and L-(+)-tartaric acid were purchased from Alfa Aesar. V_2O_5 was prepared by decomposition of NH_4VO_3 at 773 K, purchased from Sigma Aldrich. The method described in the literature for the preparation of $(TEA)_4[V_4O_8(\text{L-tart})_2]\cdot 6H_2O$ (**1·6H$_2$O**)[7] was modified according to the procedure described below, giving a **1·11H$_2$O** phase as a reaction product.

General procedure for the synthesis of phase 1·11H$_2$O

Freshly prepared V_2O_5 (0.045 g, 0.25 mmol) was dissolved in an aqueous solution of TEAOH (0.5 mL of a 2.34 mol L^{-1} solution, 1.22 mmol), and then an aqueous solution of L-(+)-tartaric acid (0.5 mL of a 1 mol L^{-1} solution, 0.5 mmol) was added to the reaction mixture. The pH of the red solution was 6.5. After this, ethanol (2.5 mL) and acetone (10 mL) were added to the reaction mixture to promote crystallization. From the reaction mixture that was kept in a refrigerator at 280 K, large red rod-like crystals of $(TEA)_4[V_4O_8(\text{L-tart})_2]\cdot 11H_2O$ (**1·11H$_2$O**) appeared after 12 h. Anal. Calcd % for $C_{40}H_{106}N_4O_{31}V_4$ (found, %): C, 35.77 (34.91); H, 7.96 (8.30); N, 4.17 (4.01); V, 15.17 (15.09). IR bands (4000–400 cm^{-1}): 3460 s, br, 3380 s, br, 3270 s, br [$\nu_{s,as}$(OH)]; 1663 vs [ν_{as}(COO^-)]; 1595 vs, 1350 m [ν_s(COO^-)]; 1296 m, 1173 s, 1097 s [ν(C–O$_h$)]; 1070 m [ν(C–O$_h$)]; 1001 s, 966 vs [ν(V=O$_t$)]; 931 w, 852 m, 822 m, 780 w, 745 s [ν_{as}(VOV)]; 656 m [ν_s(VOV)]; 634 w, 602 w, 546 s [ν(V–O$_{tart}$)]; 511 sh, 480 m, 435 m, 403 m.

Spectroscopic measurements

Attenuated total reflectance (ATR) spectra were recorded in the 4000–400 cm^{-1} range using a PerkinElmer FT-IR Frontier spectrometer. Humidity-dependent ATR measurements were recorded *in situ* using a chamber with a manual device for monitoring the relative humidity (RH) that was attached to the ATR module of the spectrometer. The relative humidity of the device was adjusted with a flow of dry or wet gas in the chamber. Temperature-dependent ATR spectra were recorded *in situ* using a hot air gun for heating. UV-vis diffuse reflectance spectra were recorded using a Shimadzu UV-Vis-NIR spectrometer (model UV-3600) equipped with an integrated sphere. The MAX-303-Compact Xenon Light source with a 300 W lamp and UV filters was used to irradiate the samples.

Thermogravimetric measurements

Thermal analysis (TG/DTA) was performed using a Shimadzu DTG-60H analyser, in the range from room temperature to 1073 K, in a stream of synthetic air at a heating rate of 2 K min^{-1}.

Electrical measurements

The current response to changes in relative humidity and temperature associated with structural transformations was monitored using a PalmSens4 potentiostat on a compressed powder samples. Ferroelectric tests were performed using a TF Analyzer 1000 at room temperature in the frequency range of 0.1–10 Hz.

Crystallographic measurements

The single-crystal X-ray diffraction data were collected by ω-scans using Cu-Kα radiation (λ = 1.54179 Å, microfocus tube, mirror monochromator) using a Rigaku XtaLAB Synergy diffractometer at 160 K. The crystal data, experimental conditions and final refinement parameters are summarized in Table S1 in the ESI.† Data reduction, including the multiscan absorption correction, was performed using the CrysAlisPRO software package.[20] The molecular and crystal structures were solved by direct methods using the program SIR2019[21] and refined by the full-matrix least-squares method based on $F2$ with anisotropic displacement parameters for all non-hydrogen atoms (SHELXL-2014/7).[22] Both programs were operating under the WinGX program package.[23] Hydrogen atoms attached to the C atoms of the $(TEA)^+$ cation and tartrate anions were treated as riding in idealized positions, with the C–H distances of 0.93 Å and displacement parameters assigned as $U_{iso}(H) = 1.2U_{eq}(C)$. Hydrogen atoms of water molecules were identified based on different Fourier maps [O–H distances were restrained to a target value of 0.85(2) Å, and the H–O–H angle to 104°]. Geometrical calculations were carried out using PLATON[24] and the figures were generated using CCDC-Mercury programs.[25] The powder X-ray diffraction (PXRD) data were collected in reflection mode using Cu-Kα radiation (λ = 1.54060 Å) using a Malvern Panalytical Empyrean diffractometer with a step size of 0.001° in a 2θ range between 5° and 60°. For *in situ* PXRD measurements, high temperature camera was used. The peak search and indexing were carried out using the TOPAS software.[26] Unit cell and profile refinements were carried out using the Pawley method.[27]

Results and discussion

Crystal transformations

The target complex salt $(TEA)_4[V_4O_8(L\text{-tart})_2]$ was prepared using a modified literature method, giving the undecahydrate complex (**1·11H$_2$O**), whereas a hexahydrate phase (**1·6H$_2$O**) was reported in a previous publication (ref. code EDAZOZ).[2,7] The two solvate phases crystallise in different crystal systems: **1·11H$_2$O** adopts the orthorhombic structure $P2_12_12_1$, while **1·6H$_2$O** has a monoclinic polar space group $P2_1$. Fig. 1, which shows a comparison between the two solvate phases, suggests that the $(TEA)^+$ cations and the $[V_4O_8(L\text{-tart})_2]^{4-}$ anions in both compounds have essentially the same geometry, with the $(TEA)^+$ cations in the **1·6H$_2$O** phase exhibiting a higher degree of thermal motion. The tetranuclear anion $[V_4O_8(L\text{-tart})_2]^{4-}$ consists of a $\{V_4O_8\}$ core, with four oxygen atoms bridging vanadium(v) ions (single bonded), four terminal oxygen atoms (double bonded) and two fully deprotonated $(L\text{-tart})^{4-}$ anions that adopt a tetradentate coordination mode to bridge metal ions and to chelate them with two hydroxyl oxygen and two carboxylic oxygen atoms. The coordination polyhedra around the vanadium(v) metal centres have a shape of a distorted square pyramid, and the overall complex anion has a boat conformation. The metal–oxygen bond lengths in the $\{V_4O_8\}$ core are in the range of 1.590(3)–1.601(2) Å for terminal oxo atoms and in the range of 1.775(2)–1.876(2) Å for bridging oxo

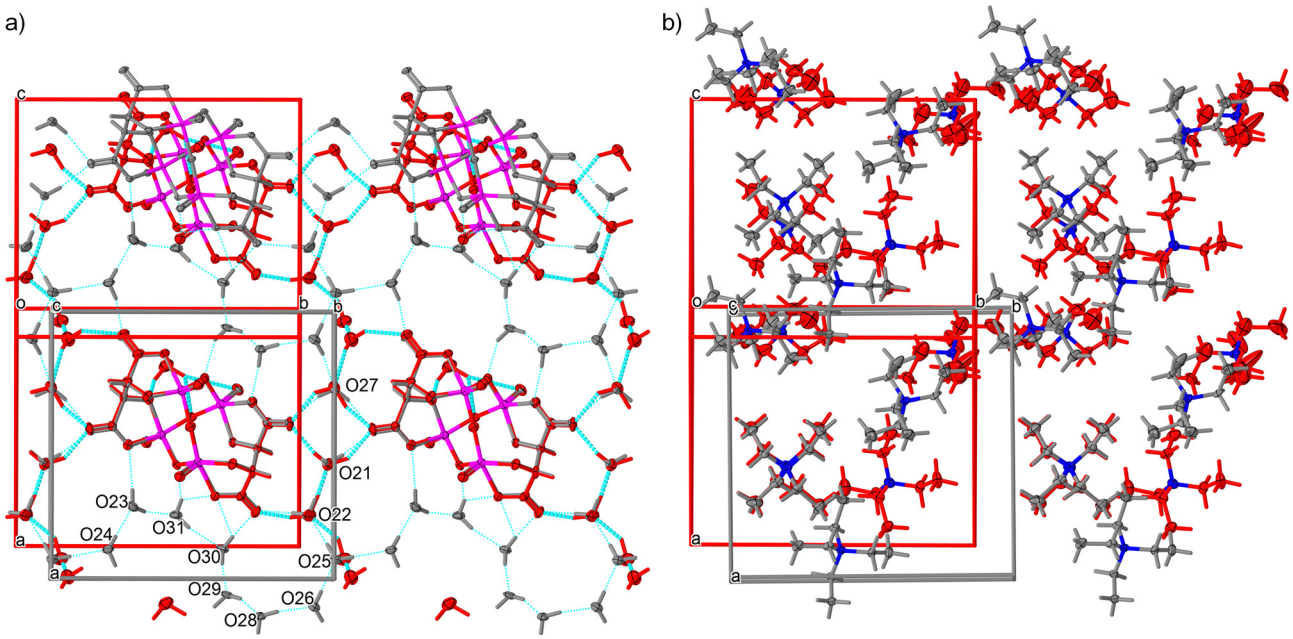

Fig. 1 Difference in crystal packing between the structure of **1·11H$_2$O** (grey) and **1·6H$_2$O** (red), showing (a) a layer with $[V_4O_8(L\text{-tart})_2]^{4-}$ anions and water molecules connected by hydrogen bonds (cyan sticks), and (b) a layer with hydrophobic $(TEA)^+$ cations.

atoms. One oxo bridge in the $\{V_4O_8\}$ core is flatter than the others, with a V–O–V angle of 170.7(1)° compared to 127.9(1), 113.6 (1) and 114.3(1)° of the other oxo bridges. The other bonds are comparable to those of the corresponding bonds in other structurally reported $[V_4O_8(\text{L-tart})_2]^{4-}$ anions.[2,7–10]

A comparison of the two phases from single-crystal XRD measurements at low temperatures shows that the **1·11H$_2$O** phase has an evidently larger unit cell than **1·6H$_2$O** (~380 Å^3, 6% volume of the unit cell), as expected due to 5 more water molecules in the crystal structure. The water molecules together with the $[V_4O_8(\text{L-tart})_2]^{4-}$ anions form a two-dimensional hydrogen bonded layer in both structures (Fig. 1a). Geometrical parameters describing hydrogen bonding are given in the ESI† (Tables S3 and S4) for both phases. When the relative humidity level is below 60%, water molecules O23, O24, O28, O30 and O31 are released from the structure of **1·11H$_2$O** (Fig. 1a). The positions of water molecules O21, O22, O25 and O27 only slightly change. During transformation, the water molecule O29 is being moved for about 3.2 Å to a new position very close to the $[V_4O_8(\text{L-tart})_2]^{4-}$ anion in the structure of **1·6H$_2$O**. The difference between two structures in terms of hydrogen bonding is that in **1·11H$_2$O** all water molecules participate in the supramolecular 2D hydrogen bonding layer (12 bonds of the donor–donor–acceptor type), forming an 8-membered cooperative infinite O–H···O–H···O–H chain. In **1·6H$_2$O**, there are no cooperative hydrogen bonding chains, and most of the interaction are the donor–donor–acceptor type, except one water molecule that is forming a discreet donor–donor type of bond with one $[V_4O_8(\text{L-tart})_2]^{4-}$ anion. Both structures contain two hydrophobic layers; in **1·11H$_2$O**, they are moderately twisted, whereas in **1·6H$_2$O** one layer is almost planar and the other forms a zigzag wrinkled sheet. In this type of structural rearrangement, the distances between the nearest $(TEA)^+$ cations are shorter in **1·11H$_2$O** than those in the **1·6H$_2$O** phase. A detailed study and comparison of the two structures show that the arrangement of the cations and anions is very similar and that even water molecules occupy very close positions with respect to the complex anions.

Similarities in the crystal structures of **1·11H$_2$O** and **1·6H$_2$O** are a direct indication that these two compounds are linked by certain solid-state transformations. Indeed, *in situ* PXRD measurements (Fig. 2) have shown that **1·11H$_2$O** is stable only in a humid atmosphere (RH ~ 60%), while a decrease in humidity leads to the elimination of 5 water molecules and consequently a symmetry breaking to the polar phase **1·6H$_2$O**. Furthermore, heating of **1·6H$_2$O** leads to the formation of three different crystalline phases at 313, 341 and 373 K, respectively. According to the PXRD data and profile fitting analysis, these phases are the result of the elimination of water molecules from the crystal structure (see Fig. S1–S5, ESI†). The relevant structural parameters (unit cell and space groups) of the five different hydrates and the dehydrated phase of the studied complex salt are listed in Table 1 (more detailed in Table S2, ESI†). The schematic representation of the structural transformations under specific conditions is shown in Scheme 2. Under humid conditions, the **1·6H$_2$O** phase shows an affinity for the uptake of water molecules from air, undergoing a structural transformation from the monoclinic $P2_1$ phase to the orthorhombic $P2_12_12_1$ phase. Mild heating from room temperature to 314 K leads to a new structural transformation within the same space group triggered by the release of a water molecule, indicating a very flexible structural rearrangement of the constituting units in this tetraethyammonium (L-tartrato)oxovanadium(V) system. Water molecules also play a role in the next structural transformation, which occurs upon heating to 341 K, when the release of three water molecules triggers the structural change from the $P2_1$ phase to the $C2$ phase. Upon further heating to 373 K, the complete loss of the water molecules occurs and the dehydrated phase **1** is formed. After thermal treatment at 423 K, the compound becomes dark brown in colour and based on the

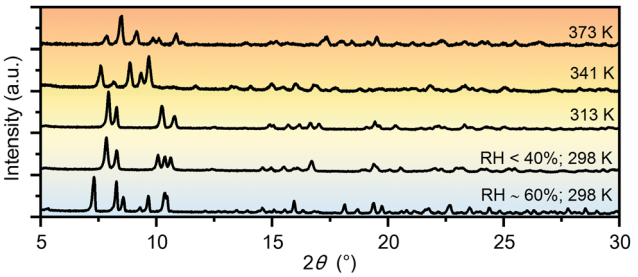

Fig. 2 PXRD patterns of the different hydrate phases and the dehydrated phase of the complex salt $(TEA)_4[V_4O_8(\text{L-tart})_2]$ (**1**) measured during heating and exposure to different relative humidities.

Table 1 Unit cell parameters and space group of the various hydrate phases and the dehydrated phase of the complex salt $(TEA)_4[V_4O_8(\text{L-tart})_2]$ (**1**)

Phase	**1·11H$_2$O**	**1·6H$_2$O**	**1·5H$_2$O**	**1·2H$_2$O**	**1**
T/K	298	298	313	341	373
M_r/g mol^{-1}	1343.04	1252.97	1234.95	1180.90	1144.87
Space group	$P2_12_12_1$	$P2_1$	$P2_1$	$C2$	$P2$
a/Å	13.331(1)	12.292(1)	12.051(1)	23.946(3)	11.720(2)
b/Å	14.150(1)	14.023(1)	13.983(2)	12.401(1)	14.095(3)
c/Å	34.466(2)	18.377(1)	18.600(2)	19.470(2)	16.786(3)
α/°	90	90	90	90	90
β/°	90	108.929(4)	109.430(5)	103.387(10)	94.720(14)
γ/°	90	90	90	90	90
Z	4	2	2	4	2
V/Å^3	6501.2(6)	2996.1(4)	2955.8(5)	5624.5(1)	2763.6(10)

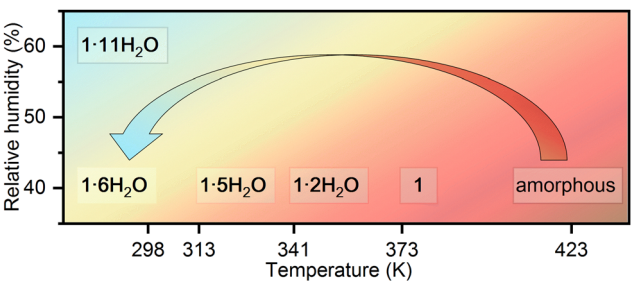

Scheme 2 Schematic representation of the structural transformations in the complex salt $(TEA)_4[V_4O_8(\text{L-tart})_2]$ (**1**) triggered by the change in humidity and temperature.

PXRD pattern appears to be an amorphous phase, showing only three broad humps (Fig. S6, ESI†). Interestingly, the amorphous phase can be recovered to a **1·6H$_2$O** crystal phase when exposed to air with a RH of > 40% at room temperature. After about 2 days in humid air, the amorphous phase absorbs water vapour from the air, causing it to dissolve and then recrystallize (see Fig. S6, ESI†).

Our findings on the dynamics of structural transformations in this (L-tartrato)oxovanadium(V) complex salt are somewhat consistent with previous observations on the stability of tartrates,[1,10,14] *i.e.*, how difficult it is to find and control the experimental conditions under which these materials exhibit adequate stability, uniform composition and consequently reproducible properties.

These results are also confirmed by the alternating isothermal and dynamic TG/DTA analysis (Fig. S8, ESI†), which show that phase **1·6H$_2$O** loses water molecules in three successive steps during heating. While phase **1·6H$_2$O** is heated to 313 K, one water molecule is eliminated (Fig. S8, ESI†), leaving the **1·5H$_2$O** phase (weight loss for 1H$_2$O: w_{calc} = 1.44%; w_{exp} = 1.29%). The next step, corresponding to the elimination of three water molecules, begins with further heating and ends at 341 K, resulting in a **1·2H$_2$O** phase (weight loss for 3H$_2$O: w_{calc} = 4.32%; w_{exp} = 5.15%). Further heating to 373 K gives the dehydrated phase **1** (weight loss for 2H$_2$O: w_{calc} = 2.87%; w_{exp} = 2.08%).

The reversible structural transformations in the complex salt (TEA)$_4$[V$_4$O$_8$(L-tart)$_2$] triggered by humidity and temperature changes, in addition to PXRD, were monitored *in situ* by ATR spectroscopy (Fig. 3). The intensity of the bands associated with the O–H stretching vibration [ν(OH)] of the lattice water molecules (range 3650–3250 cm^{-1})[28] decreases as the structure is transformed from **1·11H$_2$O** to **1·6H$_2$O**, and further from **1·6H$_2$O** to **1·2H$_2$O**. The position of these bands also changes: in **1·11H$_2$O** there are three medium broad bands at 3460, 3380 and 3270 cm^{-1}; in **1·6H$_2$O** two broad bands at 3390 and 3280 cm^{-1}; and in **1·2H$_2$O** three bands at 3517, 3368 and 3264 cm^{-1}. The tartrate ligands form hydrogen bonds with the surrounding water molecules, so the intensity and positions of the bands related to the vibrations of [ν_{as}(CO)] (range 1680–1590 cm^{-1}) and [ν_s(CO)] (range 1390–1330 cm^{-1}) are also affected by these structural transformations. For example, in **1·11H$_2$O**, a strong band related to the asymmetric C–O stretching vibration of the tartrate ligands, located at 1663 cm^{-1}, shifts to lower energies at 1628 and 1623 cm^{-1}, in **1·6H$_2$O** and **1·2H$_2$O**, respectively. In contrast, the positions and intensities of the bands associated with the symmetric and asymmetric stretching vibrations of the –CH$_2$ and –CH$_3$ groups of the (TEA)$^+$ cations appearing at 2989, 2956, 2923 and 2903 cm^{-1} show no change with temperature or humidity. This is also true for other deformation vibrations originating from the (TEA)$^+$ cations, such as the bending of the –CH$_3$ group or the scissoring of the –CH$_2$ group, which appear as bands at 1483, 1455 and 1439 cm^{-1}.[29] This is consistent with the structural studies that have shown that the cations arrange in separate hydrophobic layers and form only weak interactions with the anions. Another indication of the structural transformations is the red shift of the strongest band in the spectra corresponding to the vibrations of the terminal V=O bond, from 966 to 951 cm^{-1}.[30]

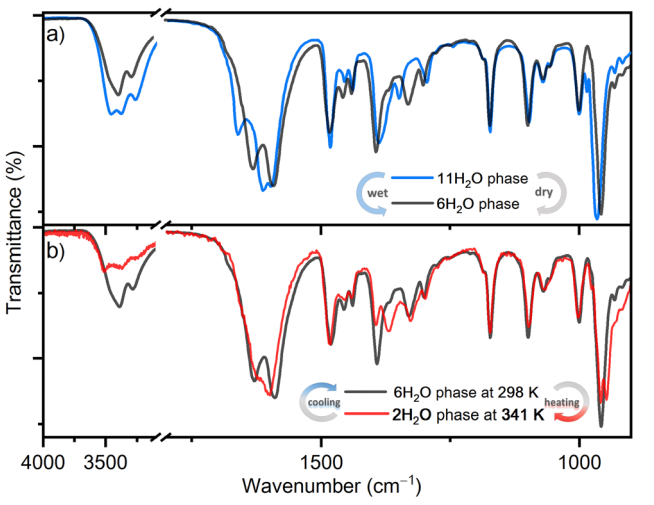

Fig. 3 ATR spectra recorded *in situ* following transformations: (a) from the initial **1·11H$_2$O** phase to the **1·6H$_2$O** phase and backward induced by a change in the humidity at room temperature; (b) from the **1·6H$_2$O** phase to the **1·2H$_2$O** phase and backward induced by a change in the temperature.

Electrical properties

The observed structural transformations in the complex salt (TEA)$_4$[V$_4$O$_8$(L-tart)$_2$] involving dehydration/rehydration processes have a significant impact on the electrical properties of the material. The reversible transformation from the **1·11H$_2$O** phase to the **1·6H$_2$O** phase is dependent on the specific RH conditions and shows a prominent current response to a change in the RH (range from 5% to 60%). Humidity sensing experiments were performed by passing alternately dry and humid air at room temperature (293–298 K) over a 0.22 μm thick pellet attached to silver wires with a silver paste. The current response to changes in the relative humidity is shown in Fig. 4. As can be seen, the current response is less than 40 nA at low humidity (below 10% RH). An increase in humidity results in an order of magnitude increase in the current

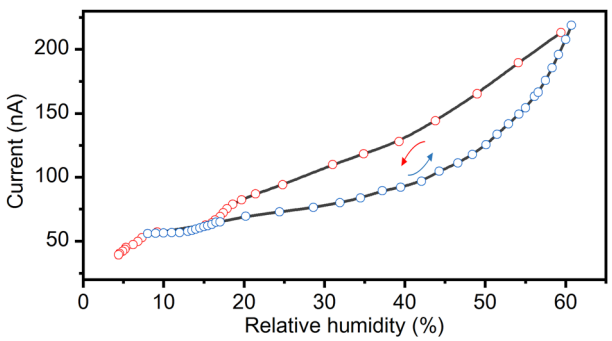

Fig. 4 Changes in the current response (conductivity) at 295 K and 1 V with an increase and a decrease in the relative humidity, induced by the reversible structural conversion of **1·11H$_2$O** to **1·6H$_2$O**.

response, up to a maximum value of 0.22 μA at 60% RH. The observed humidity-induced electrical responses are related to the formation of phase **1·6H$_2$O** under dry conditions, and phase **1·11H$_2$O** at a RH of ∼ 60%. The formation of these phases was confirmed by *in situ* PXRD and ATR measurements (Fig. 2 and 3). Exposure of the **1·6H$_2$O** phase to humid air at room temperature induces the uptake of 5 additional water molecules, leading to a solid-state transformation from the polar $P2_1$ phase to the non-polar $P2_12_12_1$ phase (**1·11H$_2$O**). The higher current response of the non-polar **1·11H$_2$O** phase is a consequence of the cooperative and infinite hydrogen bonding chains in the structure, which promote the proton conductivity of the material. The small hysteresis that exists between the drying and wetting processes is related to the dynamics of the solid-state transformations. The reproducibility between drying/wetting cycles is very good, and multiple cycles can be performed on a single pressed pellet. However, the pellet is not stable for measurements at a RH above 70% due to hygroscopicity. The observed hygroscopicity at high RH can be used as a self-recovery process, as the material dissolves at high RH and recrystallizes when the RH falls below 50% (see Fig. S6 with PXRD patterns in the ESI†).

As already mentioned, the complex salt of $(TEA)_4[V_4O_8(L\text{-tart})_2]$ has a room temperature hexahydrate phase, **1·6H$_2$O**,belonging to the polar $P2_1$ space group, which indicates that it is a potential ferroelectric material. The polarization–electric field (*P*–*E*) measurements at room temperature (295 K) and a RH of < 5% in a low-frequency electric field of 0.1–0.3 Hz confirmed the occurrence of the ferroelectricity in the **1·6H$_2$O** phase. To exclude the non-switching contributions (dielectric capacitance and leakage current) in this compressed ferroelectric powder sample, a positive up-negative-down (PUND) method with a double triangular voltage pulses was used.[31–34] The typical rectangular polarization hysteresis loop as a function of the electric field (*P*–*E*) is shown in Fig. 5 along with the current density *versus* the electric field (*J*–*E*) peak, confirming the macroscopic ferroelectric response due to the intrinsic spontaneous polarization. The saturation of the spontaneous polarization (P_s) value under these conditions is about 0.20 μC cm^{-2} with a low coercive electric field (E_c) of 0.7 kV cm^{-1}. These results are very similar to those of single-crystal potassium sodium L-tartrate tetrahydrate (P_s = 0.25 μC cm^{-2}; E_c = 0.28 kV cm^{-1}) measured at 276 K and a frequency of 50 Hz.[35] However, it has been reported that the spontaneous polarization is an one order of magnitude smaller and the coercive field is slightly larger in the compressed potassium sodium L-tartrate tetrahydrate powders compared with single-crystals.[36] Considering that our measurements were also performed on compressed polycrystalline samples, we can conclude that the overall ferroelectric performance of **1·6H$_2$O** is far better than that of a potassium sodium L-tartrate tetrahydrate. Both compounds are hydrogen-bonded tartrate-based materials with a single axis of spontaneous polarization, so a correlation can be made between them to some extent. The origin of the ferroelectricity of potassium sodium L-tartrate tetrahydrate has long been the subject of experimental and theoretical debate,[17,37,38] and it has recently been proposed that the ferroelectric-paraelectric phase transition from the monoclinic $P2_1$ to the orthorhombic $P2_12_12_1$ structure is not of the pure order–disorder type or the displacement type, but lies between the two types. The ferroelectric–paraelectric phase transition for **1·6H$_2$O** was not observed due to the limited thermal stability of the compound. Instead of transition to the non-polar paraelectric phase with increasing temperature, **1·6H$_2$O** loses water molecules of crystallization and undergoes a structural phase transition to the phase **1·5H$_2$O** at 313 K, which is transformed into the phase **1·2H$_2$O** at 341 K, and further into dehydrated phase **1** at 373 K, all belonging to the polar space groups, $P2_1$, $C2$, and $P2$, respectively.

The pentahydrate phase of the complex salt $(TEA)_4[V_4O_8(L\text{-tart})_2]$, **1·5H$_2$O** is formed after heating to 313 K. The temperature dependence of the resistivity of this phase is not linear, as can be seen in Fig. S9 (ESI†). During rapid (t = 20 s) heating to 333 K and cooling (t = 40 s) to 313 K cycles, this phase shows a significant change in resistance, as shown in Fig. 6. The experiment was performed under a constant dry air flow to maintain the relative humidity below 20% during the measurement and also to allow more efficient cooling. The sample, in the form of a 0.22 μm thick pellet attached to silver wires with a silver paste, was heated with a hot air gun. It was found that the current response increased sharply when heated and decreased when cooled. The maximum current increases from 0.062 μA at 313 K to 0.502 μA at 333 K, showing that the **1·5H$_2$O** phase has a

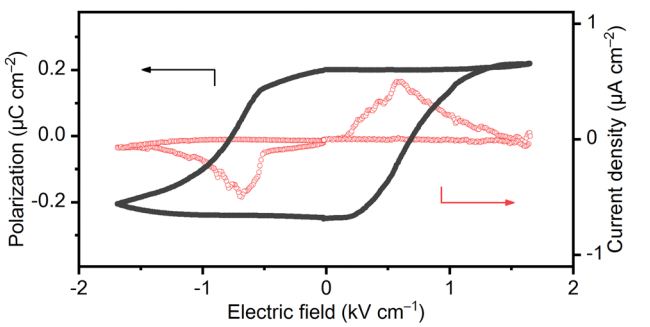

Fig. 5 Ferroelectric polarization at 295 K and RH < 5% for **1·6H$_2$O** showing *P*–*E* hysteresis loops and the corresponding current response at a 0.1 Hz switching frequency.

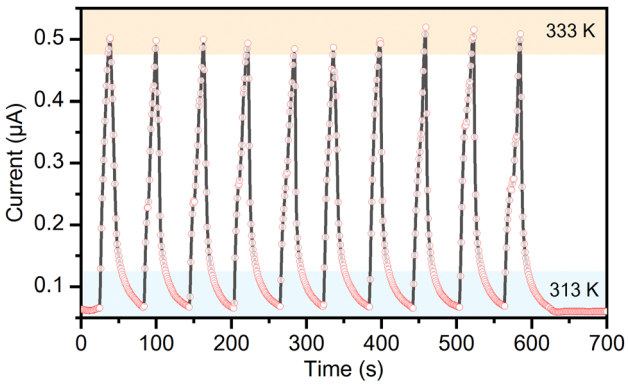

Fig. 6 Current response of the **1·5H$_2$O** phase at 10 V while switching between two heating stages at 313 K and at 333 K.

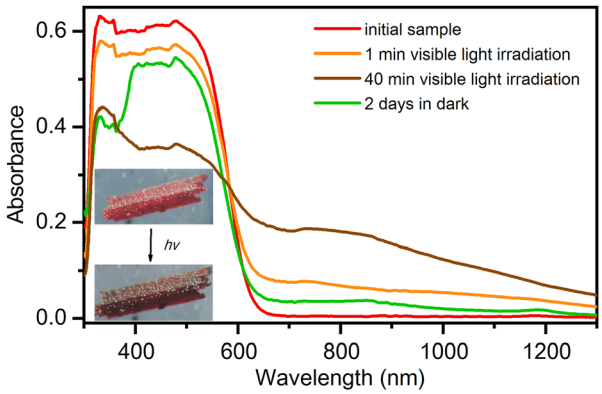

Fig. 7 Irradiation-time dependence of the UV-vis diffuse reflectance spectra of **1·6H$_2$O**. Spectra were recorded at 295 K *ex situ* at 0, 1 and 40 minutes of irradiation with a Xenon lamp (300 W, UV filter) and after a recovery period of 2 days in the dark.

negative temperature coefficient. To evaluate the sensitivity of a thermal response, the value of the temperature coefficient of resistance (TCR) was calculated using the formula TCR = $[(R - R_0)/R_0]/\Delta T$, where R is the instantaneous resistance at a measured temperature and R_0 is the original resistance.[39] The measured TCR of −4.38% K^{-1} is similar to inkjet-printed Cs_2SnI_6 thermistors (TCR = −4.95% K^{-1}),[40] and highly crystalline ferroelectric $Bi_4Ti_3O_{12}$ nanoparticles (TCR = −5.76% K^{-1}),[41] whose performance is comparable to commercial negative-temperature-coefficient thermistors fabricated on solid substrates. Phase **1·5H$_2$O** also exhibited a high thermal index of 4856 K, and a temperature sensing range of 20 K. For compound $[Pb_7I_{14}(bcbp)_2]_n$ with a metal–organic framework structure, a similar thermal index value (4671 K) was reported but with a lower temperature coefficient of resistivity (0.72% K^{-1}) and a wider operating temperature range (180 K).[42]

The **1·5H$_2$O** phase exhibits very good stability in the repeated temperature responses and the overall performance is superior to other metal–organic thermistor systems. The reason for the observed thermistor behaviour of the **1·5H$_2$O** phase could be the thermal activation of the carriers, $(TEA)^+$ cations and bulky $[V_4O_8(L\text{-tart})_2]^{4-}$ anions in this flexible molecular solid. The tartrate anions that coordinate, chelate, and bridge the vanadium ions from the inorganic $\{V_4O_8\}$ core are responsible for most of the non-covalent intermolecular interactions that govern the crystal packing of the compound. The flexibility of the crystal structure, controlled by the tartrate anions, could be one of the reasons for the observed excellent thermoelectric properties. The low energy barrier for the reversible release and uptake of water molecules from the crystalline solid-state product is a direct consequence of the flexibility of the crystal packing. Such soft materials, whose properties and sensing are based on external triggers and environments, are attracting more attention recently.[43–45]

Optical properties

Electronic spectra in the solid state, as shown in Fig. 7, were recorded for the most stable phase under ambient conditions (temperature 295 K and 40% relative humidity), the hexahydrate phase **1·6H$_2$O**. The phase **1·6H$_2$O** contains vanadium(V) centres with a d^0 electronic configuration. The strongest band in the visible part of the spectrum at 480 nm, which is also responsible for the intense red colour of the compound, is due to the ligand-to-metal charge transfer (LMCT) of the bridging oxo groups. The LMCT band decreases when the compound is exposed to visible light (generated by the 300 W xenon light source with UV filter), and crystals turn to dark brown colour. In parallel with the decrease in the intensity of the oxo-LMCT band, new absorptions can be observed in the 600–1300 nm range. The bands in this range are often associated with d–d transitions of compounds containing the oxovanadium(IV) group.[46,47] Thus, this observation suggests that vanadium(V) in the initial complex is partially reduced to vanadium(IV). When an irradiated compound is left in the dark for 2 days, it partially returns to the initial state. The recovery process can be observed first visually, by the change in the colour of the crystal from dark brown to red, and also from the electronic spectra where an increase in the LMCT band at 480 nm is observed. The self-recovery process can be sped up by exposing the irradiated material to air with high relative humidity, which induces its dissolution and recrystallization.

Another interesting feature of the obtained single-crystals of **1·11H$_2$O** is pleochroism. If the crystal is rotated for 90° under the polarised light, its colour changes from yellow to red, depending on the direction of light polarization with respect to the crystallographic axes (see Fig. S7, ESI†). This optical property is the result of crystal anisotropy and it is a rather rare phenomenon in metal–organic compounds. A similar effect is observed in recently reported bis(oxalato)chromium(III) complex salts, where crystals change the colour from purplish red to orange.[45]

Conclusion

A straightforward synthesis of the undecahydrate phase of $(TEA)_4[V_4O_8(L\text{-tart})_2]$ is reported, giving the targeted compound in high yield and a single-crystal form. The investigated compound exhibits multiple solid-state transformations triggered by humidity and temperature changes in a very narrow range, leading to the formation of different (hexa-, penta- and di-) hydrate phases and the dehydrated phase. The structural transformations were followed by *in situ* PXRD and ATR measurements, demonstrating their fast dynamics, reversibility and reproducibility. The different hydrate phases exhibit different electrical properties. The undecahydrate phase belongs to a non-polar orthorhombic $P2_12_12_1$ structure, comprising a cooperative infinite chain of hydrogen-bonded water molecules. However, the undecahydrate phase is stable only under humid conditions (RH ∼ 60%), and a decrease in humidity leads to the loss of 5 water molecules and the formation of the polar monoclinic hexahydrate phase. This phase shows a room temperature ferroelectric polarization switching of about 0.20 μC cm^{-2} at a low coercive electric field of 0.7 kV cm^{-1},

comparable to that of an archetypal ferroelectric Rochelle salt. In addition to the ferroelectric properties, the hexahydrate phase also exhibits photoresponsive behaviour, associated with the partial reduction of V(v) to V(iv) ions under visible light. Mild heating to 313 K leads to the formation of the pentahydrate phase, which has a high thermal index and a large value of the temperature coefficient of resistance, comparable to those of commercial negative-temperature-coefficient thermistors. Further heating to 341 and 373 K leads to the successive elimination of water molecules, and the formation of dihydrate and dehydrated phases, respectively. Interestingly, the material becomes amorphous after heating to 423 K and can be returned to the hexahydrate phase by exposure to humid air.

Altogether, we have shown that the system of tetraethylammonium cations and complex anions consisting of an inorganic $\{V_4O_8\}$ core chelated with fully deprotonated L-tartaric acid is a strikingly soft material whose properties and sensing can be fine-tuned by external triggers and environments, which may be of interest for use in devices.

Conflicts of interest

There are no conflicts to declare.

Acknowledgements

Financial support from the Croatian Science Foundation (UIP-2019-04-7433) is gratefully acknowledged.

Notes and references

1 M. Biver, *Inorg. Chem.*, 2021, **60**, 18360–18369.
2 C. R. Groom, I. J. Bruno, M. P. Lightfoot and S. C. Ward, *Acta Crystallogr.*, 2016, **B72**, 171–179.
3 M. Bobtelsky and J. Jordan, *J. Am. Chem. Soc.*, 1947, **69**, 2286–2290.
4 H. Sakurai, S. Funakoshi and Y. Adachi, *Pure Appl. Chem.*, 2005, **77**, 1629–1640.
5 H. Nakamura, M. Fujii, Y. Sunatsuki, M. Kojima and N. Matsumoto, *Eur. J. Inorg. Chem.*, 2008, 1258–1267.
6 T. G. Hörner and P. Klüfers, *Eur. J. Inorg. Chem.*, 2016, 1798–1807.
7 P. Schwendt, A. S. Tracey, J. Tatiersky, J. Gáliková and Z. Žák, *Inorg. Chem.*, 2007, **46**, 3971–3983.
8 J. Cao, Y. Xiong, X. Luo, L. Chen, J. Shi, M. Zhoua and Y. Xu, *Dalton Trans.*, 2018, **47**, 6054–6058.
9 P. Antal, P. Schwendt, J. Tatiersky, R. Gyepes and M. Drábik, *Transition Met. Chem.*, 2014, **39**, 893–900.
10 J. Gáliková, P. Schwendt, J. Tatiersky, A. S. Tracey and Z. Žák, *Inorg. Chem.*, 2009, **48**(17), 8423–8430.
11 J. G. Forrest and C. K. Prout, *J. Chem. Soc. A*, 1967, 1312–1317.
12 J. T. Wrobleski and M. R. Thompson, *Inorg. Chim. Acta*, 1988, **150**, 269–277.
13 Z. Sun, T. Chen, C. Ji, S. Zhang, S. Zhao, M. Hong and J. Luo, *Chem. Mater.*, 2015, **27**, 4493–4498.
14 P.-F. Li, Y. Ai, Y.-L. Zeng, J.-C. Liu, Z.-K. Xu and Z.-X. Wang, *Chem. Sci.*, 2022, **13**, 657–664.
15 J. Wu, T. Takeda, N. Hoshino and T. Akutagawa, *J. Mater. Chem. C*, 2020, **8**, 10283–10289.
16 J. Valasek, *Phys. Rev.*, 1921, **17**, 475–481.
17 F. Jona and G. Shirane, *Ferroelectric Crystals*, Dover Publications, New York, 1993.
18 H.-Y. Ye, Y. Zhang, S. Noro, K. Kubo, M. Yoshitake, Z.-Q. Liu, H.-L. Cai, D.-W. Fu, H. Yoshikawa, K. Awaga, R.-G. Xiong and T. Nakamura, *Sci. Rep.*, 2013, **3**, 2249.
19 M. Szafrański, *Angew. Chem., Int. Ed.*, 2013, **52**, 7076–7078.
20 *Agilent, CrysAlis PRO*, Agilent Technologies Ltd, Yarnton, Oxfordshire, England, 2014.
21 M. C. Burla, R. Caliandro, B. Carrozzini, G. L. Cascarano, C. Cuocci, C. Giacovazzo, M. Mallamo, A. Mazzone and G. Polidori, *J. Appl. Crystallogr.*, 2015, **48**, 306–309.
22 G. M. Sheldrick, *Acta Crystallogr., Sect. C: Struct. Chem.*, 2015, **71**, 3–8.
23 L. J. Farrugia, *J. Appl. Crystallogr.*, 2012, **45**, 849–854.
24 L. Spek, *Acta Crystallogr., Sect. D: Biol. Crystallogr.*, 2009, **65**, 148–155.
25 F. Macrae, P. R. Edgington, P. McCabe, E. Pidcock, G. P. Shields, R. Taylor, M. Towler and J. van de Streek, *J. Appl. Crystallogr.*, 2006, **39**, 453–457.
26 TOPAS version 4.2, Bruker-AXS, Karlsruhe, Germany, 2009.
27 G. S. Pawley, *J. Appl. Crystallogr.*, 1981, **14**, 357–361.
28 K. Nakamoto, *Infrared and Raman Spectra of Inorganic and Coordination Compounds*, John Wiley, New York, 6th edn, 2009.
29 S. Hajlaoui, I. Chaabane, A. Oueslati, K. Guidara and A. Bulou, *Spectrochim. Acta, Part A*, 2014, **117**, 225–233.
30 M. F. Davis, W. Levason, J. Paterson, G. Reid and M. Webster, *Eur. J. Inorg. Chem.*, 2008, 802–811.
31 S. Martin, N. Baboux, D. Albertini and B. Gautier, *Rev. Sci. Instrum.*, 2018, **88**, 023901.
32 L. Androš Dubraja, R. Kruk and T. Brezesinski, *Adv. Electron. Mater.*, 2019, **5**, 1800287.
33 U. Chowdhury, S. Goswami, D. Bhattacharya, A. Midya and P. Mandal, *Appl. Phys. Lett.*, 2016, **109**, 092902.
34 A. Puškarić, M. Dunatov, I. Jerić, I. Sabljić and L. Androš Dubraja, *New J. Chem.*, 2022, **46**, 3504–3511.
35 M. Topić, *Croat. Chem. Acta*, 1965, **37**, 245–253.
36 A. Mansingh and S. S. Bawa, *Phys. Status Solidi A*, 1974, **21**, 725–731.
37 M. I. Khan and T. C. Upadhyay, *Eur. Phys. J. D*, 2021, **75**, 211.
38 E. Suzuki and Y. Shiozaki, *Phys. Rev. B: Condens. Matter Mater. Phys.*, 1996, **53**, 5217.
39 C. Yan, J. Wang and P. S. Lee, *ACS Nano*, 2015, **9**, 2130–2137.
40 S. Li, A. Kosek, M. N. Jahangir, R. Malhotra and C.-H. Chang, *Adv. Funct. Mater.*, 2021, **31**, 2006273.
41 N. P. M. J. Raj, N. R. Alluri, A. Chandrasekhar, G. Khandelwal and S.-J. Kim, *Nano Energy*, 2019, **62**, 329–337.
42 J. Liu, X. Zhang, J. Zhang, S. Zhang, Y. Chen, H. Chen, H. Chen and M. Lin, *ACS Appl. Mater. Interfaces*, 2022, **14**(21), 24575–24582.
43 M. Kato, H. Ito, M. Hasegawa and K. Ishii, *Chem. – Eur. J.*, 2019, **25**, 5105–5112.

44 P. P. Ferreira da Rosa, Y. Kitagawa, S. Shoji, H. Oyama, K. Imaeda, N. Nakayama, K. Fushimi, H. Uekusa, K. Ueno, H. Goto and Y. Hasegawa, *Nat. Commun.*, 2022, **13**, 3660.
45 M. Dunatov, A. Puškarić, L. Pavić, Z. Štefanić and L. Androš Dubraja, *J. Mater. Chem. C*, 2022, **10**, 8024–8033.
46 A. L. Godiksen and S. Birk Rasmussen, *Catal. Today*, 2019, **336**, 45–49.
47 S. N. Choing, A. J. Francis, G. Clendenning, M. S. Schuurman, R. D. Sommer, I. Tamblyn, W. W. Weare and T. Cuk, *J. Phys. Chem. C*, 2015, **119**, 17029–17038.